Investigation of phason strains in decagonal Al-Pd-Mn single quasicrystals by means of x-ray diffraction

1998 J. Phys.: Condens. Matter 10 983

(http://iopscience.iop.org/0953-8984/10/5/008)

J. Phys.: Condens. Matter **10** (1998) 983–994. Printed in the UK PII: S0953-8984(98)86924-5

Investigation of phason strains in decagonal Al–Pd–Mn single quasicrystals by means of x-ray diffraction

Y Matsuo†, K Yamamoto† and Y Ishii‡

† Department of Physics, Nara Women's University, Nara 630, Japan

‡ Department of Materials Science, Himeji Institute of Technology, Kamigori, Hyogo 678-12, Japan

Received 18 August 1997, in final form 4 November 1997

Abstract. A careful examination of the peak profiles, peak shifts and peak separations of Bragg reflections, which are inherent in the disordering of quasicrystal, is carried out using an x-ray diffraction method for decagonal Al–Pd–Mn single quasicrystals. The full widths at half-maximum (FWHM) of the Bragg reflections along the longitudinal direction (L) have no $Q_{\parallel}$- or $Q_{\perp}$-dependence whereas those for both transverse directions, which are perpendicular to the L direction in an aperiodic plane and with a periodic axis, have linear $Q_{\parallel}$-dependence. Notable peak shifts and separations of Bragg reflections are observed. The absolute values of the shifts are found to be proportional to $Q_{\perp}$. The peak shifts and separations are analysed in terms of linear phason strains.

1. Introduction

The peak profiles, peak shifts and diffuse scattering around Bragg reflections of quasicrystals are of great interest in studies of the stability of quasicrystals and the mechanism of transformation from a quasicrystal to a crystal caused by phason strains. The first x-ray observation of diffuse scattering from single quasicrystal was carried out for an Al–Cu–Fe icosahedral quasicrystal [1]. It showed that the full widths at half-maximum (FWHM) of the Bragg reflection peaks have no $Q_{\parallel}$- and $Q_{\perp}$- dependences and that the contour maps of the diffuse scattering intensity have almost the same rhombic shape for all diffraction spots. Here $Q_{\parallel}$ and $Q_{\perp}$ are the parallel and perpendicular components of a reciprocal-lattice vector. From this observation, it was deduced that both linear phasons and quenched-in phasons are absent in the Al–Cu–Fe icosahedral quasicrystal. Recently, the diffuse scattering located close to the Bragg reflections of the Al–Pd–Mn icosahedral phase has been measured using elastic neutron scattering [2]. It was shown that the diffuse scattering has an anisotropic shape due to phason disorder, which can be explained by assuming a special configuration of phason elastic constants.

A decagonal quasicrystal has translational long-range order in one direction and orientational long-range order in a plane perpendicular to it. Thus, investigation of the decagonal phase may be more advantageous than investigation of an icosahedral phase, because of the separation of the information for a periodic direction from that for an aperiodic one. The diffuse scattering from decagonal quasicrystal was examined first for Al–Cu–Co [3]. In particular, for the Al–Ni–Co alloy, various investigations based on features such as the FWHM, diffuse satellites and diffuse scattering around the Bragg reflections were carried out using a synchrotron x-ray diffraction method [4–6]. These investigations were,

0953-8984/98/050983+12$19.50

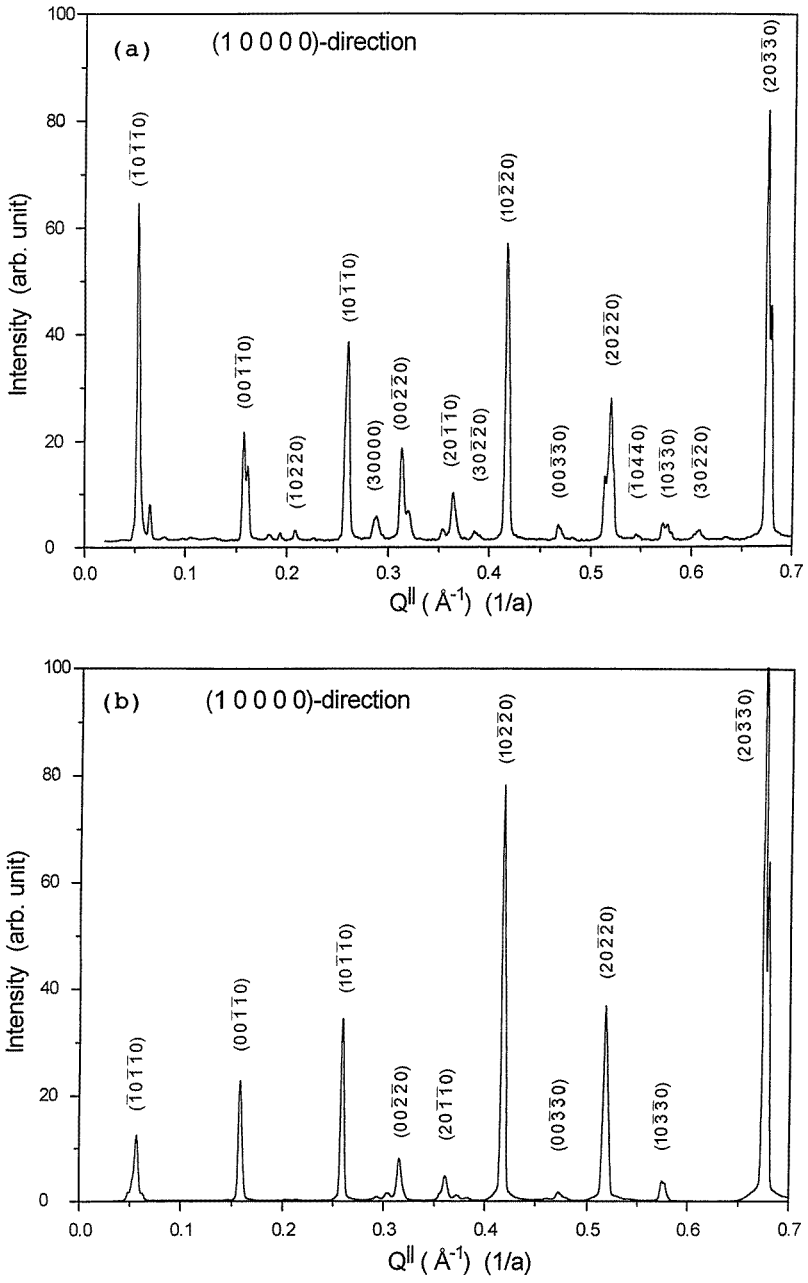

Figure 1. Line scans along the (10000) direction for type 1 (a) and for type 2 (b) structures.

however, restricted to the strong reflection peaks, and no systematic analyses, such as analysis of the $Q_{\parallel}$- and $Q_{\perp}$-dependences of the diffraction peak position and width, have been made.

In the Al–Pd–Mn alloy system, a stable decagonal phase is also formed at a composition close to $Al_{70}Pd_{10}Mn_{20}$ [7, 8]. In the electron diffraction and high-resolution electron

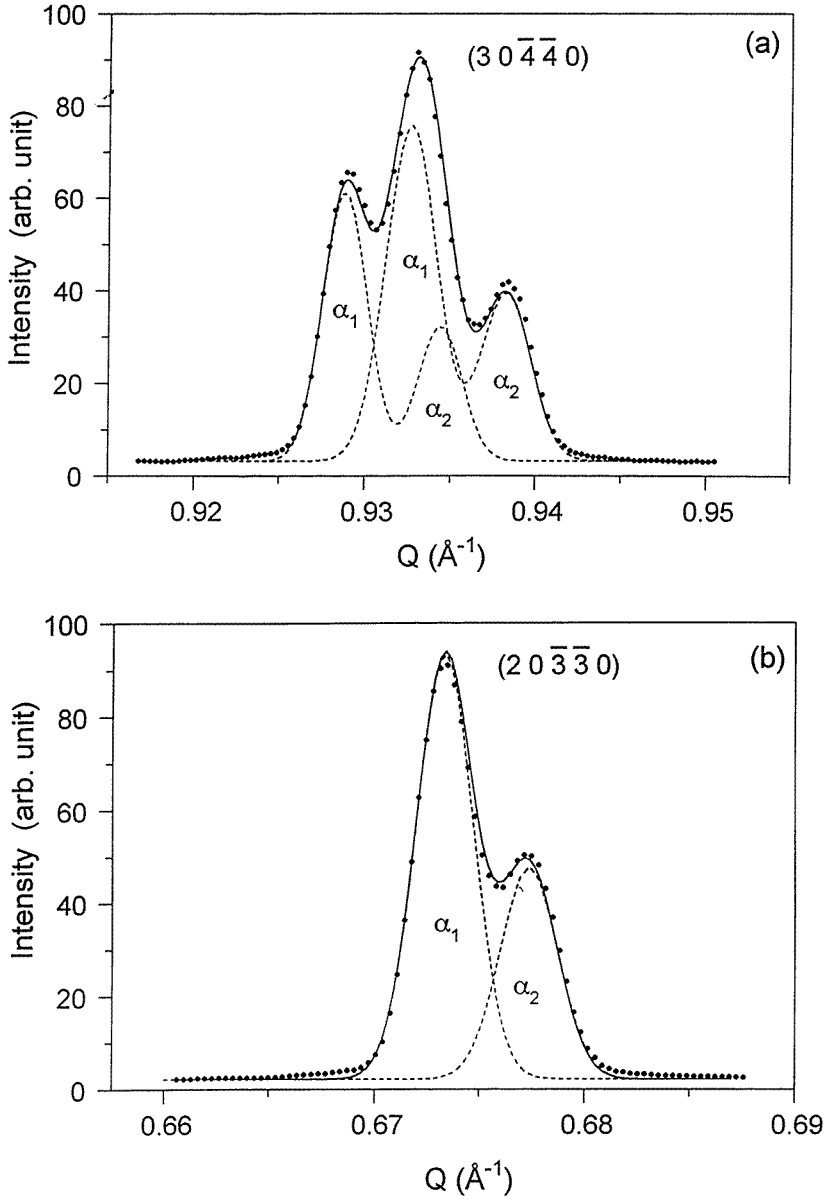

Figure 2. Peak profiles for type 1 structures along the L direction for the (30$\bar{4}\bar{4}$0) peak (a) and for the (20$\bar{3}\bar{3}$0) peak (b).

microscopy observations, linear phason strain was indicated by the shifts of the electron diffraction spots from their ideal positions and displacements of linear arrays of ring contrasts in high-resolution images [9]. An experimental study of x-ray diffraction, however, has not yet been carried out for this alloy phase because of the difficulty in making a high-quality single quasicrystal. The purpose of the present work is to investigate detailed information for the peak profile, peak shift and other properties inherent in disordering for the Al–Pd–Mn decagonal phase using an x-ray diffraction method.

2. Experimental procedure

An alloy ingot with a nominal composition of $Al_{70}Pd_{18}Mn_{12}$ was prepared by melting a mixture of pure Al, Pd and Mn metals in an Ar atmosphere using an arc furnace. This ingot was crushed into powder, put into an alumina crucible and then sealed in a quartz tube. The powder specimen was remelted at 1173 K and slowly cooled to 1073 K at a rate of 1 K min^{-1}. After its annealing at this temperature for 24 hours, the specimen was quenched in water. Needle-like single crystals with decaprismatic morphology were cut off.

X-ray diffraction experiments were carried out using Mo Kα radiation monochromated by flat HOPG with a conventional four-circle diffractometer (Rigaku AFC-5) operated at 40 kV and 20 mA. First, in order to identify the Al–Pd–Mn decagonal phase, a diffraction pattern along the longitudinal direction (L direction) was measured for many single crystals. Then, the detailed line-shape of the Bragg reflections along the L direction and along the two transverse directions which are perpendicular to the L direction in an aperiodic plane (the T1 direction) and along a periodic direction (the T2 direction) were measured in the Q-scan mode, which means that a step scan with equal intervals was carried out in reciprocal space. The Q-scans along the L, T1 and T2 directions are referred to as L, T1 and T2 scans, respectively.

The x-ray diffraction measurements were made for two kinds of diffraction geometry. One was the crystal orientation with the tenfold axis parallel to the ϕ-axis and perpendicular to a scattering plane for both L and T1 scans and the other was with the tenfold axis perpendicular to the ϕ-axis and parallel to scattering plane for the T2 scan.

In order to measure precisely both the position and the width of the diffraction peak in the L scan, which corresponds to a θ–2θ scan, high resolution was achieved using a sharp slit with horizontal width of 0.067° and a vertical width of 0.5°. The momentum resolution along the L direction is 3.3×10^{-3} Å^{-1} in this slit system. For T1 and T2 scans, which correspond to ω-scans, a square slit with horizontal and vertical widths of 0.5° was used. Two-dimensional intensity measurements were made at intervals with $Q = 0.35 \times 10^{-3}$ Å^{-1} around the Bragg reflection positions. The intrinsic beam dispersion of the present x-ray system was estimated to be 0.25° from the measurement of the (004) Bragg reflection of a Ge single crystal shaped into a sphere of 0.327 mm diameter.

3. Results

In this article, we adopt the same indexing scheme as was used by He *et al* [3], where the first five integers indicate the quasiperiodic plane and the last one indicates the periodic direction. In the present experiment, the last integer was kept at zero. Thus, only the first five integers will be used. Hereafter, we call two of the twofold symmetry axes in the quasiperiodic plane (10000) and (01001) directions, using a five-dimensional (5D) indexing scheme. If the $(20\bar{3}\bar{3}0)$ and $(021\bar{1}\bar{2})$ directions are identified with (10 0 0) and (0 6 0) for orthorhombic symmetry, we have lattice parameters $a = 1.483$ nm and $b = 1.214$ nm which correspond to the $a = 1.483$ nm and $b = 1.251$ nm for the approximant Al_3Mn orthorhombic crystal [10].

Figure 1 shows two typical diffraction patterns along the (10000) direction within the zeroth order of the quasiperiodic plane. Measurements were carried out from $Q = 0.03$ Å^{-1} to $Q = 1.12$ Å^{-1} with a step size of 0.35×10^{-3} Å^{-1} and the integral time for each step was 40 s. As shown in the figure, these peaks are very sharp, and they are indexed as the decagonal phase. But some weak peaks are split into two peaks and the behaviour of the splitting is somewhat different in figure 1(a) and figure 1(b). Hereafter, we call these

samples type 1 for (a) and type 2 for (b), respectively.

Figure 2 shows the typical peak profiles along the L direction. As can be seen in figure 2(a), the peak profile for the $(30\bar{4}\bar{4}0)$ reflection shows asymmetry or splitting even after consideration of the α_1–α_2 separation. After subtraction of the α_2-components, these peaks are divided into two symmetrical peaks, each of which is fitted by a single Gaussian function. We refer to the stronger peak as a fundamental one and the weaker one as a subpeak. For the $(20\bar{3}\bar{3}0)$ reflection, no appreciable peak splitting is observed after subtracting the α_2-component (see figure 2(b)). The peak profiles along the T1 and T2 directions are also fitted by a single Gaussian curve. After these treatments the FWHM and the peak positions are precisely determined.

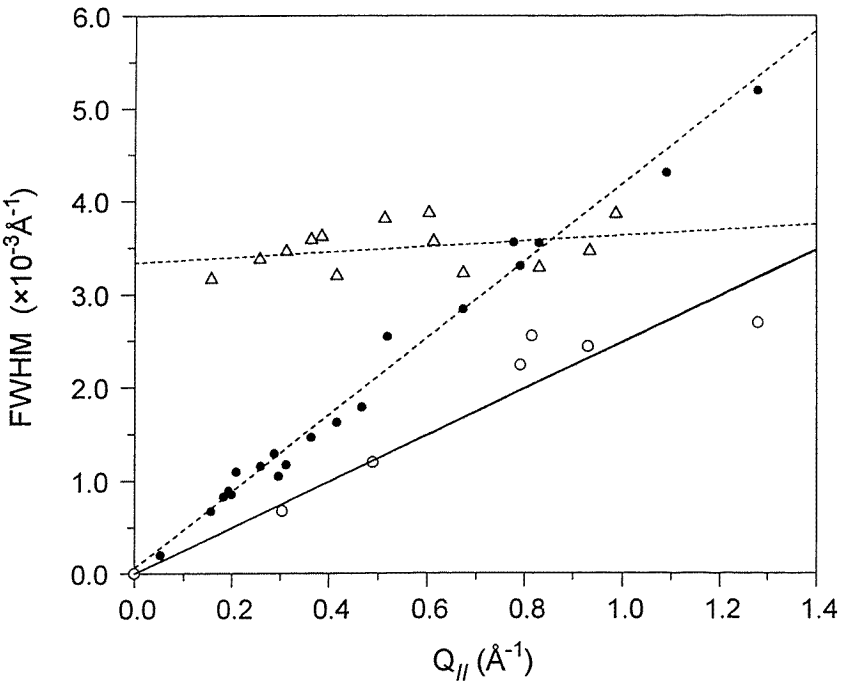

Figure 3. The FWHM as a function of $Q_\parallel$. Open triangles, filled circles and open circles denote the L, T1 and T2 directions, respectively. The solid line shows the T direction for the Ge single crystal.

The FWHM along the L, T1 and T2 directions are plotted as functions of $Q_\parallel$ in figure 3. Open triangles, filled circles and open circles denote the L, T1 and T2 directions, respectively. The solid line shows the result for the T direction for a standard Ge single crystal. From the figure it is clear that the FWHM along the L direction seems to be constant at around 3.4×10^{-3} Å^{-1}. Since the resolution for a horizontal slit corresponds to the value 3.0×10^{-3} Å^{-1} for the L direction, a substantial component is not strong enough to be detectable. On the other hand the FWHM along the T1 and T2 directions have $Q_\parallel$-linear dependence. The FWHM along the T1 and T2 directions are normally caused by the crystal mosaicity. So the distortion of mosaicity in the quasiperiodic plane is larger than that along the periodic axis, which is the same as the case for the resolution for the x-ray dispersion observed from standard Ge single crystal.

The lattice parameter in 5D space is estimated as $A_{5D} = 6.439$ Å using three strong

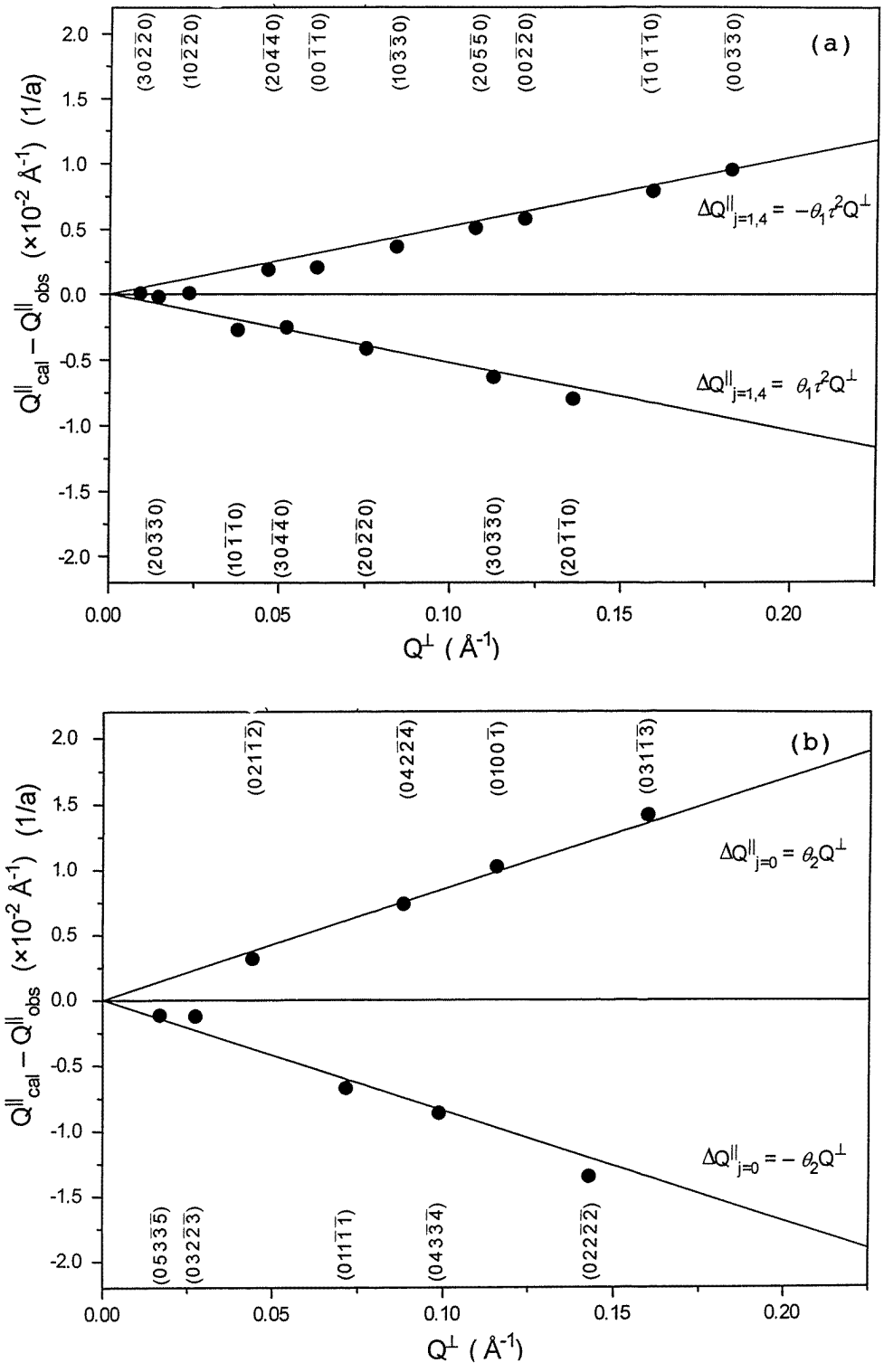

Figure 4. Peak shifts of the Bragg reflection position as functions of $Q_{\perp}$ for the (10000) direction (a) and for the (0100$\bar{1}$) direction (b).

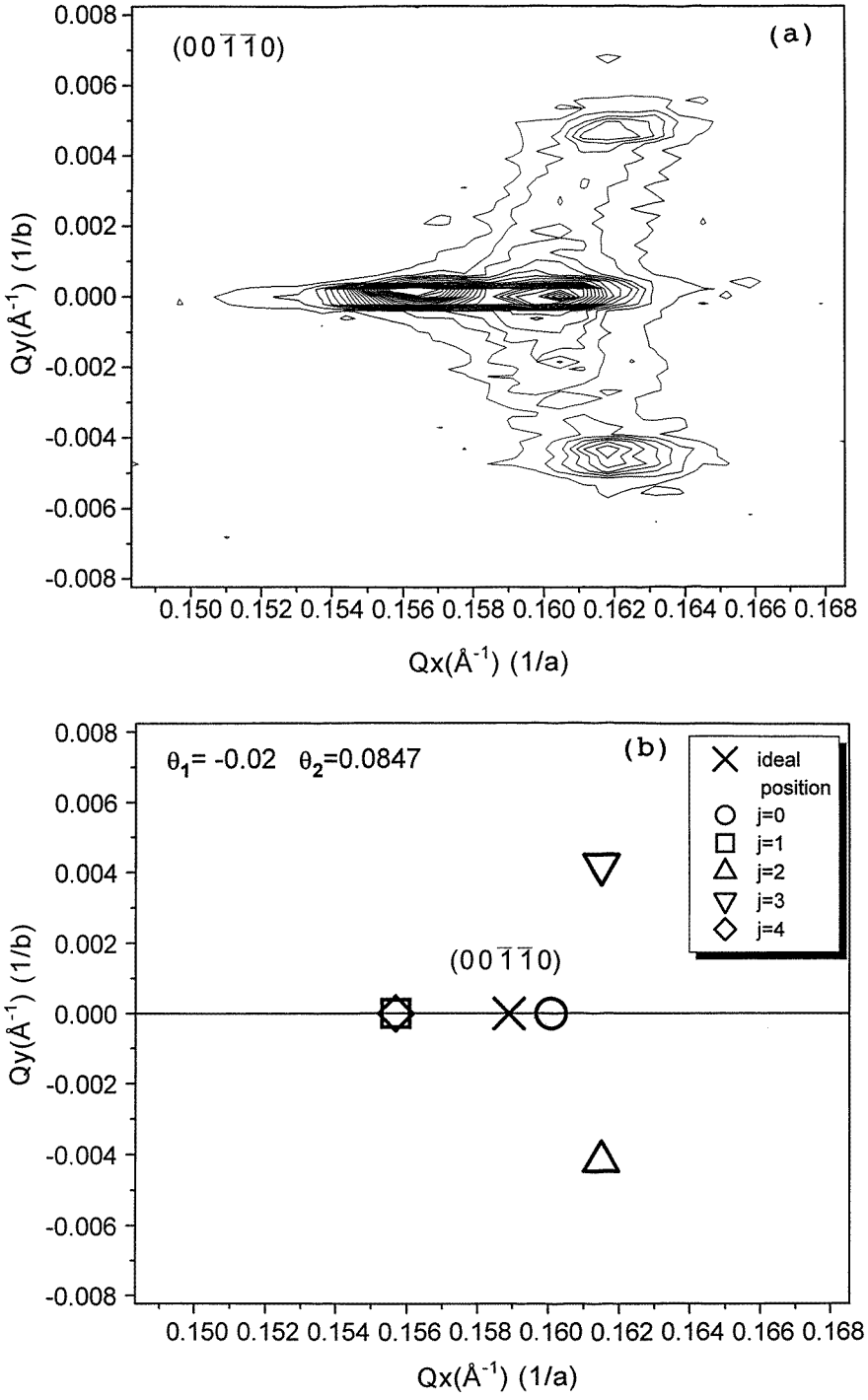

Figure 5. A two-dimensional contour map around the (00$\bar{1}\bar{1}$0) reflection for a type 1 structure (a) and a schematic illustration of the model calculation (b).

peaks indexed as $(10\bar{2}\bar{2}0)$, $(20\bar{3}\bar{3}0)$ and $(30\bar{5}\bar{5}0)$, which are reflections without splitting (see figure 2(b)). This value is similar to that, $A_{5D} = 6.313$ Å, for the decagonal Al–Cu–Co quasicrystal [3]. Using this lattice parameter, the shifts of the fundamental peaks from the ideal positions are plotted as functions of $Q_\perp$ for the type 1 sample in the (10000) and $(0100\bar{1})$ directions in figure 4. As can be seen in the figure, for both directions, the magnitudes of the shifts have $Q_\perp$-linear dependence and are divided into two groups: those with $\Delta Q_\parallel = cQ_\perp$ and those with $\Delta Q_\parallel = -cQ_\perp$ with the same constant slope c. This tendency is also observed for the type 2 samples although the slope c is less than that for the type 1 samples. Figure 5(a) shows the two-dimensional contour map around the $(00\bar{1}\bar{1}0)$ reflection for the type 1 samples. The measurement was carried out with a step size of 0.35×10^{-3} Å^{-1} for each direction and the measuring time for each step was 40 s. As can be seen in the figure, the Bragg peak is split into four peaks.

4. Discussion

Precise measurements for the peak profiles and positions of the Bragg peaks have been carried out for two types of Al–Pd–Mn decagonal quasicrystal sample. The FWHM in the L direction seems to be constant at around 3.4×10^{-3} Å^{-1} with no $Q_\parallel$- and $Q_\perp$-dependence. This means that the D phase of Al–Pd–Mn has no random phason strain or other phason disorder. This trend has also been observed for the Al–Cu–Co decagonal phase [3] though the value of 0.014 Å^{-1} was larger than that for the Al–Pd–Mn phase. The FWHM in the T1 and T2 directions, on the other hand, have small $Q_\parallel$-linear dependences and the slope for the T1 direction is larger than that for the T2 direction. These results imply that the Al–Pd–Mn single decagonal crystals are highly ordered quasicrystals with long-range correlation although the arrangement of the columnar decagonal cluster has some mosaicity in an aperiodic plane.

To understand the peak shifts in figures 3(a) and 3(b) and the peak separation in figure 5(a), we introduce a phason strain matrix as follows:

$$\mathbf{M} = \begin{pmatrix} \theta_1 & 0 \\ 0 & \theta_2 \end{pmatrix} \tag{1}$$

where the shift of a Bragg peak is given by

$$\Delta \boldsymbol{Q}_\parallel = \mathbf{M}\boldsymbol{Q}_\perp. \tag{2}$$

The phason matrix $\mathbf{M}$ and its symmetric equivalents split the $(m0\bar{n}\bar{n}0)$ reflection into five spots as follows:

$$\begin{aligned} \Delta \boldsymbol{Q}_\parallel^{j=0} &= Q_\perp(\theta_1, 0) \\ \Delta \boldsymbol{Q}_\parallel^{j=1,4} &= \frac{Q_\perp}{4}\left(-\theta_1 + \frac{\tau^2+1}{\tau}\theta_2, \pm\sqrt{\tau^2+1}(\tau\theta_1 + \tau^{-2}\theta_2)\right) \\ \Delta \boldsymbol{Q}_\parallel^{j=2,3} &= \frac{Q_\perp}{4}\left(-\theta_1 - \frac{\tau^2+1}{\tau}\theta_2, \pm\sqrt{\tau^2+1}(-\tau^{-2}\theta_1 + \tau\theta_2)\right) \end{aligned} \tag{3}$$

with $Q_\perp = \sqrt{2/5}\,2\pi/[A_{5D}(m - n/\tau)]$ and the $(0mn\bar{n}\bar{m})$ reflection given by

$$\begin{aligned} \Delta \boldsymbol{Q}_\parallel^{j=0} &= Q_\perp(0, \theta_2) \\ \Delta \boldsymbol{Q}_\parallel^{j=1,4} &= \frac{Q_\perp}{4}\left(\pm\sqrt{\tau^2+1}(\tau^{-2}\theta_1 + \tau\theta_2), \frac{\tau^2+1}{\tau}\theta_1 - \theta_2\right) \\ \Delta \boldsymbol{Q}_\parallel^{j=2,3} &= \frac{Q_\perp}{4}\left(\pm\sqrt{\tau^2+1}(\tau\theta_1 - \tau^{-2}\theta_2), -\frac{\tau^2+1}{\tau}\theta_1 - \theta_2\right) \end{aligned} \tag{4}$$

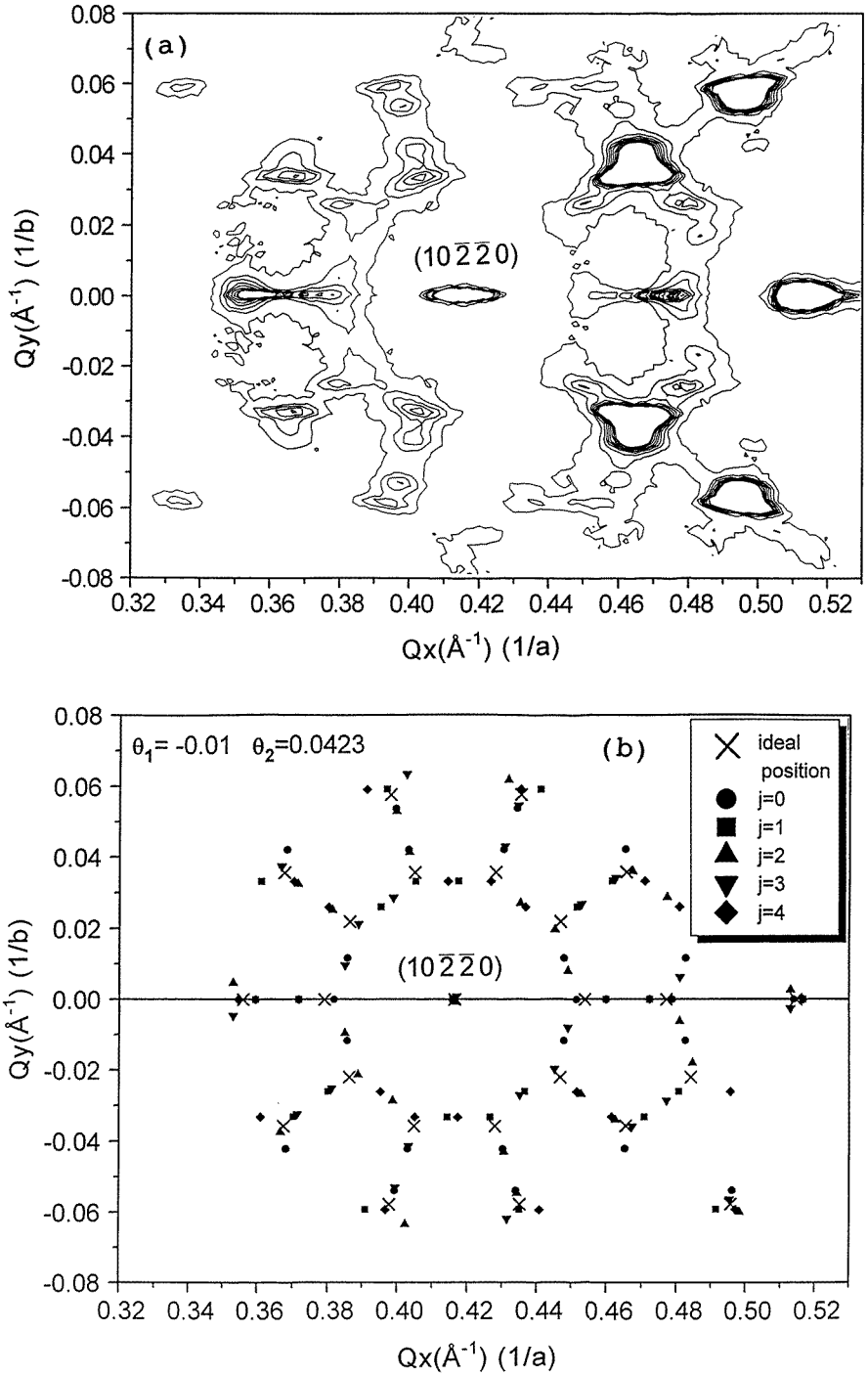

Figure 6. A two-dimensional contour map around the (10$\bar{2}\bar{2}$0) reflection for a type 2 structure (a) and a schematic illustration of the model calculation (b).

with $Q_\perp = \sqrt{2/5}\,2\pi/[A_{5D}\sqrt{\tau^2+1}(m/\tau - n)]$. Here τ is the golden mean (1.6180...).

With the special choice $\theta_2 = -\tau^3\theta_1$, two spots, with $j = 1$ and $j = 4$, split from the $(m0\bar{n}\bar{n}0)$ reflection coincide with each other and eventually we have four split peaks around the ideal position as shown in figure 5(b). Here the fundamental peak for the $(m0\bar{n}\bar{n}0)$ reflection should be identified as the overlapped peak whereas the subpeak should be identified as the $j = 0$ spot. The $(0mn\bar{n}\bar{m})$ reflection, on the other hand, splits into five peaks with the $j = 0$ spot located in the L direction. The peak shifts along the L direction for the $(m0\bar{n}\bar{n}0)$ and $(0mn\bar{n}\bar{m})$ reflections shown in figures 2(a) and 2(b) are then $\Delta Q_\parallel = \pm\tau^2\theta_1|Q_\perp|$ and $\Delta Q_\parallel = \pm\theta_2|Q_\perp|$, respectively. The values of θ_1 and the θ_2 for the type 1 sample are estimated as -0.02 and 0.085, which correspond to $-\tau^{-8}$ and τ^{-5}, respectively.

Figure 6(a) shows a two-dimensional contour plot around the $(10\bar{2}\bar{2}0)$ reflection for the type 2 sample. The intensity distribution can also be understood on the basis of the phason strain matrix (1) with $\theta_2 = -\tau^3\theta_1$. The values of θ_1 and θ_2 in this case are estimated as $-0.01 \approx -\tau^{-10}$ and $0.042 \approx \tau^{-7}$, respectively. Figure 6(b) is a schematic illustration of the peak splitting calculated by using these values. The crosses represent the ideal positions whereas the other five types of symbol denote five split spots. The agreement with the observed intensity distribution (figure 6(a)) is remarkable.

By tuning the magnitude of the phason strains, we can derive a periodic structure called the crystalline approximant [11] (see the appendix). It is interesting to note that the phason strain with $\theta_2 = -\tau^3\theta_1$ gives an orthorhombic unit cell with $a/b = \tau\sqrt{\tau^2+1} = \tan 2\pi/5$. For $\theta_1 = -\tau^{-8}$ and $-\tau^{-10}$, the lattice parameters are given by $a = \sqrt{2/5}A_{5D}(\tau^2+1)\tau^3$ and $a = \sqrt{2/5}A_{5D}(\tau^2+1)^2\tau^3$, respectively. Using an estimated value for A_{5D} (6.439 Å), we obtain $a = 62.4$ Å and 255 Å for $\theta_1 = -\tau^{-8}$ and $-\tau^{-10}$, respectively. That is, our type 1 and type 2 samples are approximant orthorhombic crystals with lattice parameters $a = 62.4$ Å, $b = 20.3$ Å and $a = 225$ Å, $b = 73.4$ Å, respectively.

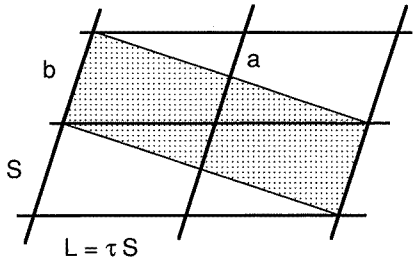

Figure 7. A parallelogram unit cell observed by Hiraga *et al* and a rectangular one (shaded).

Hiraga *et al* [9] have found microcrystalline regions with a parallelogram unit cell with edge lengths S (=2 nm) and $L = \tau S$ in high-resolution images of decagonal Al–Pd–Mn. As shown in figure 7, the unit cell can be taken as a rectangular one instead of a parallelogram, which is exactly what is found in the orthorhombic cell for $\theta_1 = -\tau^{-8}$. In addition, Beeli *et al* [12] have discovered a modification of the D phase at high temperatures. They have concluded that the modification corresponds to a pseudo-decagonal, C-centred orthorhombic approximant structure (the D_H phase) with the cell parameters $a = 2.03$ nm, $b = 6.25$ nm and $c = 1.25$ nm, established from high-resolution electron microscope observation. These cell parameters are the same as those for the approximant crystal deduced from the phason strain for the type 1 sample. Although the periodicity along the c-axis for the present family of orthorhombic approximants is different from that for $Al_{13}Fe_4$, an orthorhombic

unit cell for $Al_{13}Fe_4$, whose lattice parameters a and b are τ^2 times smaller than those for the type 1 sample (the D_H phase), is also realized by assuming a unique phason strain (1) with $\theta_2 = -\tau^3\theta_1$ and $\theta_1 = -\tau^{-4}$.

In conclusion type 1 and type 2 samples of Al–Pd–Mn decagonal alloy certainly involve phason strain with a unique configuration. The estimated phason strain is very close to that leading to crystalline approximants with a unit cell similar to the orthorhombic cell realized in $Al_{13}Fe_4$. The microcrystalline structure with a parallelogram unit cell observed by high-resolution electron microscopy [9] and an approximant phase called the D_H phase [12] are identified as type 1 samples. This suggests that the Al–Pd–Mn decagonal quasicrystal may transform to two different approximant crystals denoted as type 1 and type 2 in the present paper.

Acknowledgments

We wish to express our thanks to Professor K Hiraga, Institute for Materials Research, Tohoku University. This work was supported by a Grant-in-Aid for Scientific Research on Priority Areas, 'Phase Transformation' (No 09242102), from the Ministry of Education and Culture of Japan.

Appendix A. A crystalline approximant for the decagonal quasilattice

To describe the decagonal quasilattice, we choose three orthogonal vectors, which define the three-dimensional perpendicular space embedded in five-dimensional space, as follows:

$$\begin{aligned} \boldsymbol{e}_1^{\perp} &= \frac{1}{\sqrt{4\lambda_1^2 + 4\lambda_1 + 6}}\big(2, -(\lambda_1+1), \lambda_1, \lambda_1, -(\lambda_1+1)\big) \\ \boldsymbol{e}_2^{\perp} &= \frac{1}{\sqrt{2(\lambda_2^2+1)}}\big(0, \lambda_2, -1, 1, -\lambda_2\big) \\ \boldsymbol{e}_3^{\perp} &= \frac{1}{\sqrt{5}}\big(1, 1, 1, 1, 1\big) \end{aligned} \tag{A1}$$

where λ_1 and λ_2 should be $1/\tau$ for quasiperiodic structure. The phason strains θ_1 and θ_2 are related to λ_1 and λ_2 by

$$\theta_1 = \frac{\lambda_1 - 1/\tau}{\lambda_1 + \tau} \tag{A2}$$

$$\theta_2 = \frac{1 - \tau\lambda_2}{\lambda_2 + \tau}. \tag{A3}$$

If one replaces λ_i $(i = 1, 2)$ with an appropriate rational number p_i/q_i (p_i and q_i being integers), one obtains a crystalline approximant structure with an orthorhombic unit cell. The lattice parameters are given by

$$a = \sqrt{\frac{2}{5}}A_{5D}\,5(p_1 + q_1\tau) \tag{A4}$$

$$b = \sqrt{\frac{2}{5}}A_{5D}\,\frac{\sqrt{\tau^2+1}}{\tau}(p_2 + q_2\tau). \tag{A5}$$

If $p_1 + 3q_1 = 0 \pmod 5$, the factor 5 on the right-hand side of equation (A4) is eliminated.

The special configuration $\theta_2 = -\tau^3\theta_1$ is realized if $(\lambda_1, \lambda_2) = (F_{k+1}/F_{k+2}, G_k/G_{k+1})$ or $(G_{k+1}/G_{k+2}, F_k/F_{k+1})$ where F_k is a Fibonacci number ($F_{k+1} = F_k + F_{k-1}$ with $F_0 = 0$, $F_1 = 1$) and $G_k = F_{k-1} + F_{k+1}$. It is straightforward to check that $a/b = \tau\sqrt{\tau^2 + 1}$. In particular, $\theta_1 = -\tau^{-8}$ and $\theta_1 = -\tau^{-10}$ are realized if $(\lambda_1, \lambda_2) = (4/7, 1/2)$ and $(3/5, 4/7)$, respectively.

References

[1] Mori M, Ishimasa T and Kasiwase T 1991 *Phil. Mag. Lett.* **64** 49
[2] De Boissieu M, Boudard M, Hennion B, Bellissent R, Kycia S, Goldman A, Janot C and Audier M 1995 *Phys. Rev. Lett.* **75** 89
[3] He Y, Yan X, Egami T, Poon S J and Shiflet G J 1992 *Phil. Mag. Lett.* **66** 241
[4] Hradil K, Proffen T, Frey F, Eichhorn K and Kek S 1995 *Phil. Mag. Lett.* **71** 199
[5] Kalning M, Press W and Kek S 1995 *Phil. Mag. Lett.* **71** 341
[6] Hradil K, Proffen T, Frey F, Kek S, Krane H G and Wroblewski T 1995 *Phil. Mag.* B **71** 955
[7] Beeli C, Nissen H U and Robadey J 1991 *Phil. Mag. Lett.* **63** 87
[8] Hiraga K, Sun W, Lincoln F J, Kaneko M and Matsuo Y 1991 *Japan. J. Appl. Phys.* **30** 2028
[9] Hiraga K, Lincoln F J, Sun W and Matsuo Y 1993 *Phase Transitions* **44** 163
[10] Hiraga K, Kaneko M, Matsuo Y and Hashimoto S 1993 *Phil. Mag.* B **67** 193
[11] Ishii Y 1991 *Proc. China–Japan Seminar on Quasicrystals* (Singapore: World Scientific) p 196
[12] Beeli C, Stadelmann P, Lück R and Gödecke T 1995 *Proc. Int. Conf. on Aperiodic Crystals (Aperiodic 94)* (Singapore: World Scientific) p 361